Journal of Applied Mechanics and Technical Physics, Vol. 43, No. 1, pp. 93–102, 2002

CRYSTALLIZATION DYNAMICS OF A LIQUID METAL DROP IMPINGING ONTO A MULTILAYERED SUBSTRATE

M. R. Predtechensky,[1] A. N. Cherepanov,[2] V. N. Popov,[2] and Yu. D. Varlamov[1]

UDC 532.501.32:535.347:535.52

Thermal and hydrodynamic processes that occur during impingement of a liquid metal drop onto a multilayered substrate are numerically studied. The mathematical model is based on the Navier–Stokes equations for an incompressible liquid and on substrate and drop heat-transfer equations that take into account the surface-tension forces and metal solidification. The effect of the impact velocity, initial drop diameter, metal overheating, and temperature and thermophysical characteristics of the substrate on the morphology of the solid drop, its height, contact-spot diameter, and total solidification time was examined numerically. The simulation results are found to be in satisfactory agreement with experimental data.

Introduction. Thermal and hydrodynamic phenomena that occur during impingement of a liquid drop onto a solid surface is a subject of considerable interest because of their increasing importance in advanced applications where the spreading of a liquid over a surface is accompanied by heat transfer and phase transition. The novel technology for producing microelectronic components known as the solder-drop-printing technique is an example for this [1, 2]. The central point in this technology is deposition of liquid solder drops 40–100 μm in diameter onto microchip terminal pads, where the drops solidify to be subsequently used for mounting microelectronic components on the substrate.

Impingement of liquid metal drops (with a typical volume of the order of 10^{-12} liter) onto a cool substrate is rather a complex process in which a liquid with a free surface spreads over a solid body. This process involves considerable local deformations of substances, heat transfer, and phase transition. Depending on deposition conditions and on particular properties of substrate and drop materials, liquid flows of various types may develop in the drop, from slow capillary spreading of the liquid over the substrate surface to rapid smashing of drops against the substrate, followed by their fractionation.

In the technique under consideration, a typical velocity of liquid drops is 1–10 m/sec, which corresponds to mean Reynolds and Weber numbers ($1 < \mathrm{Re} < 2000$ and $1 < \mathrm{We} < 100$, respectively). This range of conditions seems to be a most complex one since, in this case, along with the influence of inertial and viscous forces, the effect of the surface-tension force becomes substantial.

For micron-size droplets, the characteristic spreading, oscillation, viscous-deformation, cooling, and solidification times are comparable and normally fall within the range of several microseconds. That is why experimental studies of rapid processes in a drop face serious methodical and technical difficulties. In this situation, numerical modeling becomes an effective research tool. Investigation into the dynamics of the above-indicated phenomena, in particular, temperature fields and crystallization-front velocity, is of obvious interest.

To facilitate mathematical treatment of the deformation and crystallization dynamics of a drop after its impingement onto a substrate, some simplifying assumptions were used in previous studies. For instance, Harlow and Welch [3] chose to ignore the effect of viscosity and surface tension. Tarapaga and Szekely [4] developed a numerical model that described the deformation of the free surface of a drop on a flat surface under isothermal

[1]Kutateladze Institute of Thermal Physics, Siberian Division, Russian Academy of Sciences, Novosibirsk 630090. [2]Institute of Theoretical and Applied Mechanics, Siberian Division, Russian Academy of Sciences, Novosibirsk 630090. Translated from Prikladnaya Mekhanika i Tekhnicheskaya Fizika, Vol. 43, No. 1, pp. 112–123, January–February, 2002. Original article submitted March 14, 2001; revision submitted July 2, 2001.

0021-8944/02/4301-0093 $27.00

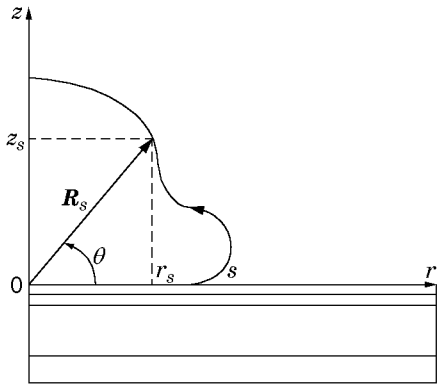

Fig. 1. Schematic of a deforming drop after its impingement onto a multilayered substrate.

conditions in the perfect-liquid approximation. Fedorchenko [5] studied numerically the drop spreading over a surface and conductive–convective heat transfer during impingement of a cylindrical drop onto a solid substrate. It was shown that two stages may be distinguished in the drop-substance collision process: 1) instantaneous impact acting upon the liquid volume; 2) forced spreading of the viscous liquid over the substrate. Fedorchenko [5] gave a detailed analysis of hydrodynamic phenomena that occur in a drop after its impact spreading over the substrate.

Using the Lagrangian representation of convective heat-transfer equations and the finite-element approach to solve them, Zhao et al. [6] developed a computer code that allowed them to examine the dynamics of a viscous metal flow in a drop after its impingement onto a substrate under the conditions without melt crystallization. This model was used by Waldvogel and Polikakos [2] to study hydrodynamic and crystallization processes in a liquid metal drop after its impingement onto a multilayered substrate. In their study, both the viscosity and the action of capillary forces at the free surface of the drop were taken into account. Nonetheless, the use of the finite-element approach made necessary extensive preliminary manipulations causing considerable loss of computer time. In addition, in solving the Stefan problem by introducing an effective heat capacity, Waldvogel and Polikakos [2] treated the latent crystallization heat as uniformly distributed over the whole temperature range considered. The latter seems to be a factor responsible for the observed decrease in the total solidification time with increasing drop overheating [2].

In the present simulations, an implicit finite-difference scheme was used, which included an iteration algorithm for solving the system of algebraic equations at each time step. The free surface of the drop was marked with particles-markers. The crystallization heat was assumed to be "smeared" in a narrow temperature interval around the equilibrium crystallization point. As a result, the solidification time was found to vary in proportion to overheating.

The adequacy of the numerical model and the approximations used were tested by comparing predicted values with experimental data. A detailed analysis of the effect of process parameters on the final shape of the drops was performed.

Physical Statement of the Problem. We study the dynamics of a liquid metal drop after its impingement onto a flat solid surface. We assume that a spherically symmetrical liquid drop impinges, at a certain velocity, onto a wettable rigid substrate. The trajectory of the drop is normal to the substrate surface, and the initial substrate temperature is lower than the crystallization point of the drop material. After the collision, the drop surface starts deforming, and an internal liquid flow develops in the drop (Fig. 1). As a result of thermal interaction, the liquid inside the drop gets cooled down to a certain critical temperature, and the overcooled metal layers solidify. Two types of solidification are possible: 1) volume solidification; 2) layer-by-layer solidification. The first type is the case if the whole liquid contained in the drop volume is overcooled down to a certain critical state, after which solid nuclei appear in the melt. The process may take either homogeneous or heterogeneous path. The latter possibility is more probable since actual alloys normally contain nondissolved microparticles that act as nucleation centers. Then, the nuclei formed further grow in size releasing the crystallization heat. During this period, the hydrodynamic processes in the drop rapidly decay owing to an abrupt increase in the apparent viscosity of substances (both of the liquid and crystals). The morphology of the solid drop correlates with the shape the drop acquires by the beginning of solidification.

Crystallization of the second type is characterized by the formation of a solid metal crust at the spot where the melt immediately contacts the substrate surface, the cooling there being most rapid and the formation of nucleation centers on the surface microroughness possible. During continuous cooling of pure metals and eutectic alloys, a macroscopically smooth crystallization front steadily propagates upward, separating out the already solidified metal from the liquid one. In this case, the liquid drop may evolve on the solid crust formed by metal crystallization. The velocity of the crystallization front and the dynamics of the liquid part of the drop determine the morphology of the drop after its complete solidification.

It should be noted that the quantitative description of solidification with due account for volume nucleation is difficult because of the lack of many data, required for calculations, on physical, chemical and kinetic parameters of nonequilibrium crystallization of high-velocity ($v_0 \geqslant 100$ m/sec) liquid-alloy drops, for which the cooling rate is normally higher than 10^5 K/sec [7]. In applying solder drops onto substrates in microelectronic technology, moderate impact velocities, $v_0 = 1$–10 m/sec, are normally used, the drop diameters being $d_0 = 40$–100 μm. The cooling rate under such conditions is usually lower than 10^5 K/sec. Therefore, to adequately describe crystallization of pure metals and eutectic alloys (for instance, Sn + Pb), one may use the Stefan-problem approximation, assuming that the temperature at the solid–liquid interface coincides with the equilibrium solidification point, the crystallization front is macroscopically smooth, and the nucleation in the liquid metal may be ignored.

Viscous-Fluid Dynamic Equations. To numerically study the dynamics of a liquid drop after its impingement onto a flat solid surface, we use the Navier–Stokes equations for a viscous incompressible fluid, assuming the flow in the drop to be laminar and the values of the thermophysical parameters of the fluid to be constant and equal to their mean values in the temperature range under consideration. With allowance for the assumptions used, the equations of the fluid flow in the axial coordinate system shown in Fig. 1 (r, z, and θ are the radial, axial, and azimuthal coordinates, respectively) have the form [8]

$$\rho\Big(\frac{\partial u}{\partial t} + u\,\frac{\partial u}{\partial r} + v\,\frac{\partial u}{\partial z}\Big) - \frac{1}{r}\,\frac{\partial}{\partial r}\,(r\sigma_{rr}) - \frac{\partial \sigma_{rz}}{\partial z} + \frac{\sigma_{\theta\theta}}{r} = 0; \tag{1}$$

$$\rho\Big(\frac{\partial v}{\partial t} + u\,\frac{\partial v}{\partial r} + v\,\frac{\partial v}{\partial z}\Big) - \frac{1}{r}\,\frac{\partial}{\partial r}\,(r\sigma_{zr}) - \frac{\partial \sigma_{zz}}{\partial z} + \rho g = 0; \tag{2}$$

$$\frac{1}{r}\,\frac{\partial}{\partial r}\,(ru) + \frac{\partial v}{\partial z} = 0, \tag{3}$$

where ρ is the density of the fluid, g is the free-fall acceleration, u and v are the radial and axial components of the velocity vector; the stress tensors $\sigma_{\theta\theta}$, σ_{rr}, $\sigma_{zr} = \sigma_{rz}$, and σ_{zz} are given by the relations

$$\sigma_{\theta\theta} = -p + p_a + \frac{2\mu u}{r}, \qquad \sigma_{rr} = -p + p_a + 2\mu\,\frac{\partial u}{\partial r},$$

$$\sigma_{zr} = \sigma_{rz} = \mu\Big(\frac{\partial u}{\partial z} + \frac{\partial v}{\partial r}\Big), \qquad \sigma_{zz} = -p + p_a + 2\mu\,\frac{\partial v}{\partial z}$$

(p is the pressure inside the liquid drop, p_a is the atmospheric pressure, and μ is the fluid viscosity).

Passing in (1)–(3) to dimensionless quantities and performing some rearrangements with allowance for the above relations, we write the system of equations of interest as

$$\frac{1}{x}\,\frac{\partial}{\partial x}\Big(x\,\frac{\partial P}{\partial x}\Big) + \frac{\partial^2 P}{\partial y^2} + \frac{1}{x}\,\frac{\partial^2 (xU^2)}{\partial x^2} + \frac{2}{x}\,\frac{\partial^2 (xUV)}{\partial x \partial y} + \frac{\partial^2 V^2}{\partial y^2} = 0,$$

$$\frac{\partial V}{\partial \tau} + \frac{\partial V^2}{\partial y} + \frac{1}{x}\frac{\partial (xUV)}{\partial x} + \frac{\partial P}{\partial y} - \frac{1}{\mathrm{Re}}\Big[\frac{1}{x}\,\frac{\partial}{\partial x}\Big(x\,\frac{\partial V}{\partial x}\Big) + \frac{\partial^2 V}{\partial y^2}\Big] + \frac{1}{\mathrm{Fr}} = 0, \tag{4}$$

$$\frac{\partial V}{\partial y} + \frac{1}{x}\,\frac{\partial (xU)}{\partial z} = 0,$$

where $\tau = tv_0/d_0$, $x = r/d_0$, $y = z/d_0$, $U = u/v_0$, $V = v/v_0$, $P = p/(\rho v_0^2)$, $\mathrm{Re} = v_0 d_0/\nu$ is the Reynolds number, $\mathrm{Fr} = v_0^2/(gd_0)$ is the Froude number, $\nu = \mu/\rho$ is the kinematic viscosity, d_0 is the initial drop diameter, and v_0 is the impact velocity.

System (4) is solved with the dimensionless boundary conditions

$$\begin{aligned} U=0,\ V=-1,\ P=4/\mathrm{We} \qquad & \text{for } \tau=0,\\ U=0,\ \frac{\partial V}{\partial x}=0,\ \frac{\partial P}{\partial x}=0 \qquad & \text{for } x=0,\\ U=0,\ V=0 \qquad & \text{for } y=\xi(x,t),\ \xi(x,0)=0, \end{aligned}$$

where $\mathrm{We}=\rho v_0^2 d_0/\sigma$ is the Weber number and $\xi(x,t)$ is the solidification front.

The last relations is supplemented by the relations at the free surface of the liquid particle:

$$\begin{aligned} \Big(P-\frac{2K}{\mathrm{We}}-\frac{2}{\mathrm{Re}}\,\frac{\partial U}{\partial x}\Big)n_x-\frac{1}{\mathrm{Re}}\Big(\frac{\partial U}{\partial y}+\frac{\partial V}{\partial x}\Big)n_y=0,\\ \Big(P-\frac{2K}{\mathrm{We}}-\frac{2}{\mathrm{Re}}\,\frac{\partial V}{\partial y}\Big)n_y-\frac{1}{\mathrm{Re}}\Big(\frac{\partial U}{\partial y}+\frac{\partial V}{\partial x}\Big)n_x=0. \end{aligned} \tag{5}$$

Here n_x and n_y are the components of a unit vector normal to the free surface of the drop, along the x and y axes, respectively, and the dimensionless curvature of the drop surface is given by the relation [6]

$$K=\frac{x_s^2(x_s'y_s''-y_s'x_s'')+[(x_s')^2+(y_s')^2]x_sy_s'}{2x_s^2[(x_s')^2+(y_s')^2]^{3/2}},$$

where the prime denotes the derivative with respect to the dimensionless arc length $S=s/d_0$ and $x_s=r_s/d_0$ and $y_s=z_s/d_0$ are the dimensionless projections of the vector $\boldsymbol{R}_s/d_0$ onto the r and z axes, respectively (Fig. 1).

Heat-Transfer Equations. We determine the change in the temperature fields in the drop–substrate system from the solution of the conjugate heat-transfer problem posed both in the liquid and solid phases of the drop, which undergoes solidification, and in the substrate. We take into account the liberation of the latent crystallization heat during the phase transition by introducing an effective heat capacity [9].

We write the heat-transfer equations in the liquid part of the drop ($i=1$), in the layer that has already solidified ($i=2$), and in the substrate ($i=3$) in the following dimensionless form:

$$\begin{aligned} c_{\mathrm{eff}}\Big(\frac{\partial\theta}{\partial\tau}+U\,\frac{\partial\theta}{\partial x}+V\,\frac{\partial\theta}{\partial y}\Big)=\frac{1}{\mathrm{Pe}_1}\Big[\frac{1}{x}\,\frac{\partial}{\partial x}\Big(x\,\frac{\partial\theta}{\partial x}\Big)+\frac{\partial^2\theta}{\partial y^2}\Big],\\ c_{\mathrm{eff}}\,\frac{\partial\theta}{\partial\tau}=\frac{1}{\mathrm{Pe}_2}\Big[\frac{1}{x}\,\frac{\partial}{\partial x}\Big(x\,\frac{\partial\theta}{\partial x}\Big)+\frac{\partial^2\theta}{\partial y^2}\Big],\qquad \frac{\partial\theta}{\partial\tau}=\frac{1}{\mathrm{Pe}_3}\Big[\frac{1}{x}\,\frac{\partial}{\partial x}\Big(x\,\frac{\partial\theta}{\partial x}\Big)+\frac{\partial^2\theta}{\partial y^2}\Big], \end{aligned} \tag{6}$$

Here $\mathrm{Pe}_i=d_0v_0/a_i$ is the Peclet number, $\theta=T_i/T_{\mathrm{eq}}$ and $\tau=tv_0/d_0$ are the dimensionless temperature and time, respectively, $a_i=\lambda_i/(c_i\rho_i)$ is the thermal diffusivity of the ith medium, and λ_i, ρ_i, and c_i are the thermal conductivity, density, and heat capacity of the medium, respectively. The effective heat capacity c_{eff} is given by the relations

$$c_{\mathrm{eff}}=\begin{cases} 1, & \theta>1+\Delta\theta/2,\\ 1+\mathrm{St}/\Delta\theta, & 1-\Delta\theta/2\leqslant\theta\leqslant 1+\Delta\theta/2,\\ c_2/c_1, & \theta<1-\Delta\theta/2, \end{cases} \tag{7}$$

where $\mathrm{St}=æ/(c_1T_{\mathrm{eq}})$ is the Stefan number, $\Delta\theta=\Delta T/T_{\mathrm{eq}}$ is the dimensionless temperature interval over which the phase transition is "smeared" [9], $æ$ is the latent crystallization heat, and T_{eq} is the equilibrium crystallization point.

Equations (6) should be supplemented with the following boundary conditions.

1. Initial values of the drop and substrate temperatures:

$$\theta_1|_{\tau=0}=\theta_{10},\qquad \theta_3|_{\tau=0}=\theta_{30}. \tag{8}$$

2. Adiabaticity condition at the free surface of the drop:

$$\bar\lambda_i\Big(\frac{\partial\theta_1}{\partial x}\,n_x+\frac{\partial\theta_1}{\partial y}\,n_y\Big)=0. \tag{9}$$

3. Condition of heat transfer between the drop and the substrate:

$$\bar\lambda_i\,\frac{\partial\theta_i}{\partial y}\Big|_{y=0+}=\lambda_3\,\frac{\partial\theta_3}{\partial y}\Big|_{y=0-}=\mathrm{Bi}(\theta_i-\theta_3). \tag{10}$$

Here $\bar{\lambda}_i = \lambda_i/\lambda_1$ ($i = 1$ for $\theta > 1$ and $i = 2$ for $\theta < 1$), $\mathrm{Bi} = kd_0/\lambda_1$ is the Biot number, $k = \Big(\sum\limits_j \dfrac{\delta_{sj}}{\lambda_{sj}}\Big)^{-1}$ is the coefficient of substrate-to-particle heat transfer through a clad coating (if the substrate is a multilayered one), and δ_{sj} and λ_j are the thickness and thermal conductivity of the jth sublayer, respectively.

4. Conditions of heat transfer at the lower, side, and upper non-wetted substrate surfaces, respectively:

$$\frac{\partial\theta}{\partial y}\Big|_{y=-\bar{L}} = 0, \qquad \frac{\partial\theta}{\partial x}\Big|_{x=x_3} = 0, \qquad \frac{\partial\theta}{\partial y}\Big|_{y=0} = 0. \tag{11}$$

Here $\bar{L} = L/d_0$ and $x_3 = r_3/d_0$ (L and r_3 are the thickness and radial dimension of the substrate; $r_3 \gg d_0$). For a polymer substrate, instead of the first condition of (11), we assume that $\theta_3|_{y=-\bar{L}} = \theta_m$, where θ_m is the dimensionless ambient temperature.

5. Symmetry condition at the y axis in the drop and substrate:

$$\frac{\partial\theta_i}{\partial x}\Big|_{x-0} = 0, \qquad i = 1, 2, 3. \tag{12}$$

The heat-transfer equations (6) with the boundary conditions (7)–(12), together with the Navier–Stokes equations for the liquid part of the particle (4), govern the drop cooling and solidification process.

Brief Description of the Numerical Algorithm. The numerical algorithm was based on a finite-difference approximation of the Navier–Stokes and heat-transfer equations with an implicit scheme of order $O(\tau, h)$ [10]. The region occupied by the unsteady melt flow was marked with successively enumerated particles-markers located along the drop contour and moving at the local fluid velocity [3]. To satisfy the monotonicity condition for the finite-difference scheme, the spatial derivatives in the inertial terms were approximated with due regard for the sign of velocity in a vicinity of each nodal point of the computational grid. The diffusion terms were substituted with their second-order difference analogs. In this approach, no limits were imposed by Reynolds numbers on the algorithm stability.

Having determined the velocity field, we calculated the temperature field in the drop and substrate according to Eqs. (5) and (6). The thermal problem is to be solved in two conjugated computational domains, in the drop and in the substrate. To match the temperature fields in the two domains, no more than three iterations were sufficient. The new coordinates of the markers, r_m^{n+1} and z_m^{n+1}, at the $(n+1)$th time step were calculated by the relations

$$r_m^{n+1} = r_m^n + u_m^n \tau_{n+1}, \qquad z_m^{n+1} = z_m^n + v_m^n \tau_{n+1}, \qquad m = 1, \ldots, M(t_n).$$

Here u_m^n and v_m^n are the particle velocities determined in accordance with the mean local velocities in a small vicinity of each of the markers and $M(t_n)$ is the number of markers at the time t_n. At each time step, we had to either remove or add some part of markers, in order to obtain their uniform distribution over the drop contour, and re-enumerate them. Throughout the whole computational domain, a spatial grid $h_x = h_y = 0.01$ was used. At the moment t_{n+1}, the time step τ_{n+1} was calculated by the formula

$$\tau_{n+1} = \min\{h_x, h_y\}/K_0 \max_m\{|u_m^n|, |v_m^n|\}, \qquad K_0 = 20.$$

Following [9], we chose the region over which the boundary between the phases was "smeared" so that the region included two or three nodes of the spatial grid. This could be achieved through preliminary estimation of typical temperature gradients. In the computer program, the temperature interval ΔT was chosen automatically. It should be noted that, in the calculations, the mean value of this parameter was 5°C.

At each time step, we solved the systems of algebraic equations using an iterative procedure. The computations were terminated on reaching the relative error of 0.002.

Results and Discussion. The model was tested for adequacy by comparing the calculated values with the experimental data obtained using the procedure described in [11]. Liquid drops of various diameters with different initial temperatures and impact velocities were deposited onto substrates with the help of a specially designed drop generator [11]. The final shape of the drops after their solidification was analyzed on a scanning electron microscope. The processes that occurred during the impingement of the microdrops onto the surface were visualized with the help of a superhigh-speed video-camera equipped with a microscope attachment and a stroboscopic system, which ensured microsecond time resolution. The inaccuracy in visualizing the spreading stages of deposited drops was ± 5 μsec; its value depended primarily on the drop-velocity fluctuations during the ejection of the drops from the generator. As the drop material, both in the experiment and computations, we used a tin-lead eutectic (63% Sn + 37% Pb). In examining the effect of heat-transfer conditions on the evolution of drops, two types of substrates were used.

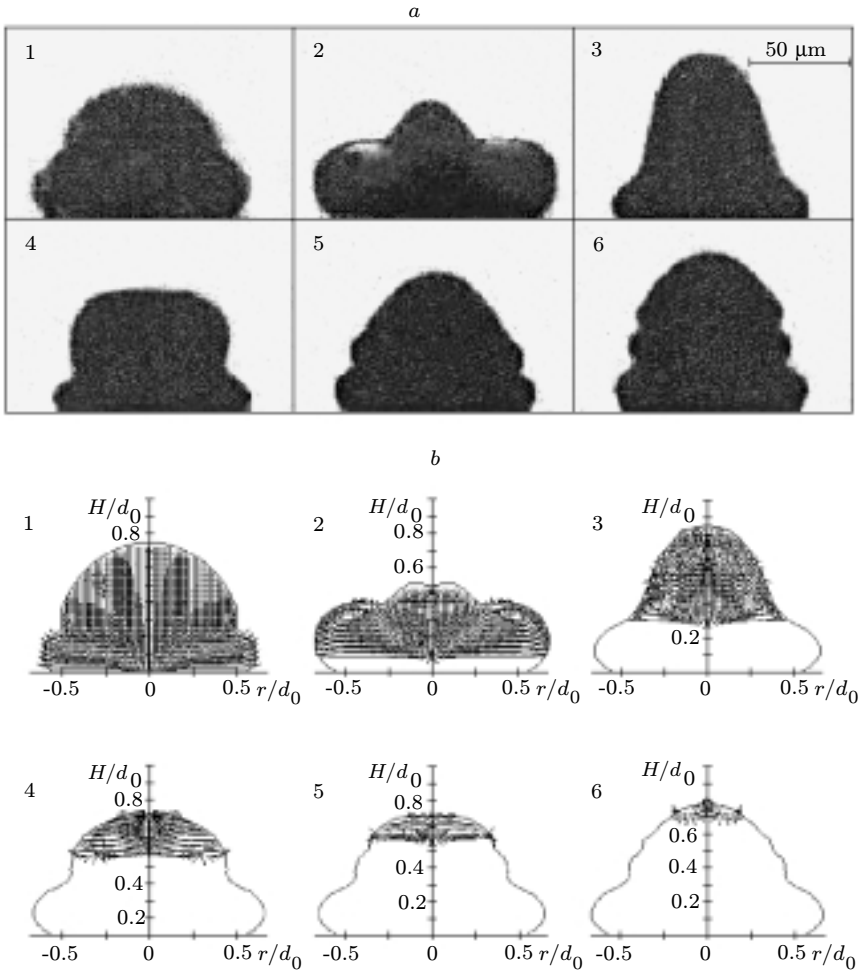

Fig. 2. Experimental (a) and computed (b) shapes of the drop after its impingement onto the copper substrate for $t = 10$ (1), 30 (2), 50 (3), 70 (4), 100 (5), and 120 μsec (6) ($d_0 = 68$ μm, $v_0 = 1.8$ m/sec, $T_0 = 240°$C, and $T_s = 50°$C).

Type 1. A 300 μm-thick copper plate placed on a polymeric base and clad from above with two metal layers (nickel lower layer of thickness $\delta_{\text{Ni}} = 0.25$ μm and gold upper layer of thickness $\delta_{\text{Au}} = 0.1$ μm). The melt cooling was assumed to occur due to heat accumulation solely by the copper layer, the two clad coatings were considered as thermal resistances, and the polymeric base was a thermal insulator. Accordingly, the adiabaticity condition was adopted at the interface between the copper plate and the polymeric base.

Type 2. A 25 μm-thick polymeric substrate with a gold coating ($\delta_{\text{Au}} = 0.1$ μm). In this case, a constant temperature was set at the lower surface. The gold layer was considered as a thermal resistance. The following values of the thermophysical parameters of the (63% Sn + 37% Pb) drop and substrate materials (copper and polymer) [2, 12, 13] were used: for the liquid phase of the drop, $\lambda = 25$ W/(m·K), $c = 238$ J/(kg·K), $\rho = 8218$ kg/m^3, $\sigma = 0.345$ N/m, $\mu = 2.62 \cdot 10^{-3}$ kg/(m·sec), $æ = 42 \cdot 10^3$ J/kg, and $T_{\text{eq}} = 456$ K, for the solid phase of the drop, $\lambda = 48$ W/(m·K), $c = 176$ J/(kg·K), and $\rho = 8218$ kg/m^3, for copper, $\lambda = 397$ W/(m·K), $c = 391$ J/(kg·K), and $\rho = 8900$ kg/m^3, and for polymer $\lambda = 0.26$ W/(m·K), $c = 1570$ J/(kg·K), and $\rho = 1924$ kg/m^3.

The proposed model was tested for adequacy by comparing the drop shapes computed for different times after the drop impingement onto the copper substrate with the experimental data previously reported in [11]. Figure 2 shows the experimentally determined and computed shapes of the drop, together with the velocity fields in its liquid part for different moments. It follows from Fig. 2 that the agreement between the experimental and predicted data is satisfactory (the difference is 10–20%). The predicted data show that the predominant part of the drop solidifies already by the moment $t = 100$ μsec after the collision at a velocity of 1.8 m/sec, whereas the upper part of the

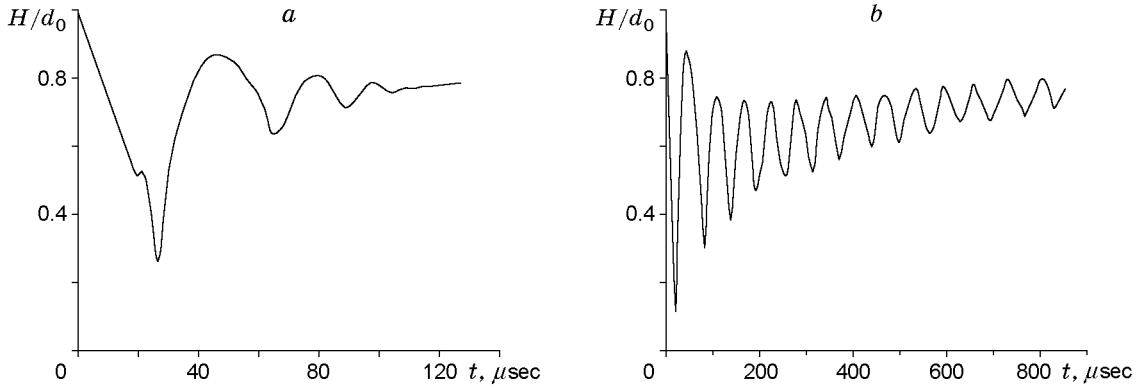

Fig. 3. Dynamics of drop-vertex oscillations after the collision of the drop with the copper substrate ($v_0 = 1.8$ m/sec) (a) and polymeric substrate ($v_0 = 3$ m/sec) (b) for $T_0 = 240°$C and $T_s = 50°$C.

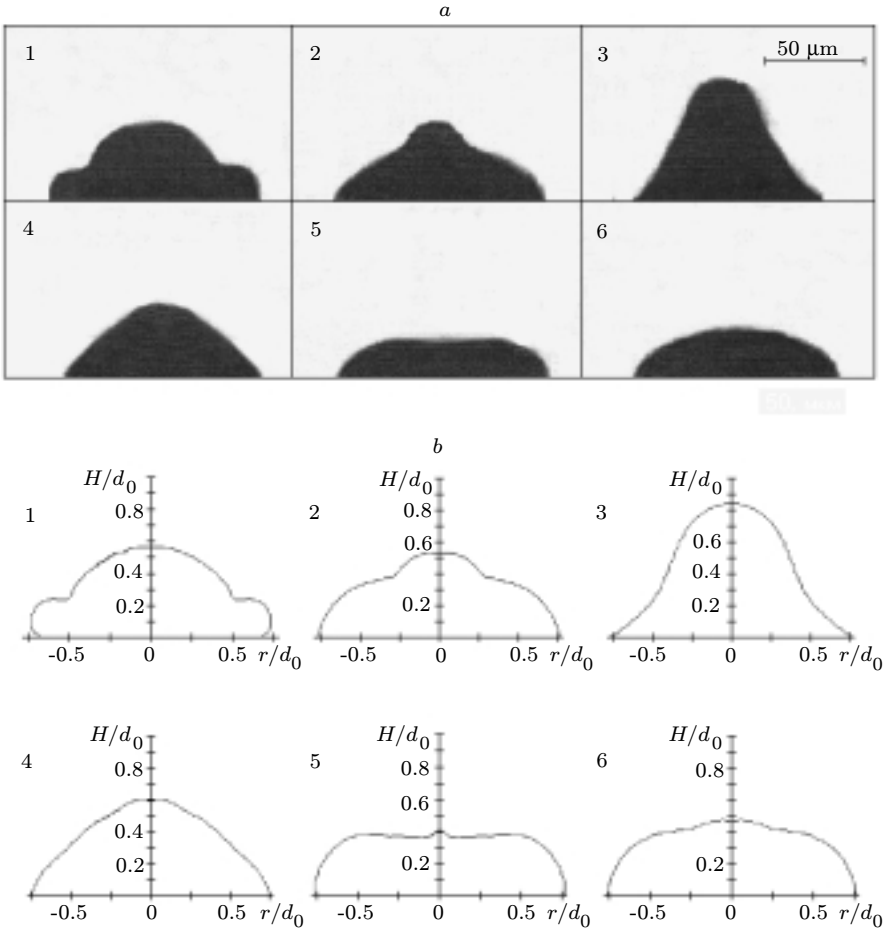

Fig. 4. Experimentally determined (a) and computed (b) shapes of the drop after its collision with the polymeric substrate ($d_0 = 62.5$ μm, $v_0 = 3$ m/sec, $T_0 = 240°$C, and $T_s = 50°$C) for $t = 10$ (1), 30 (2), 50 (3), 70 (4), 80 (5), and 90 μsec (6).

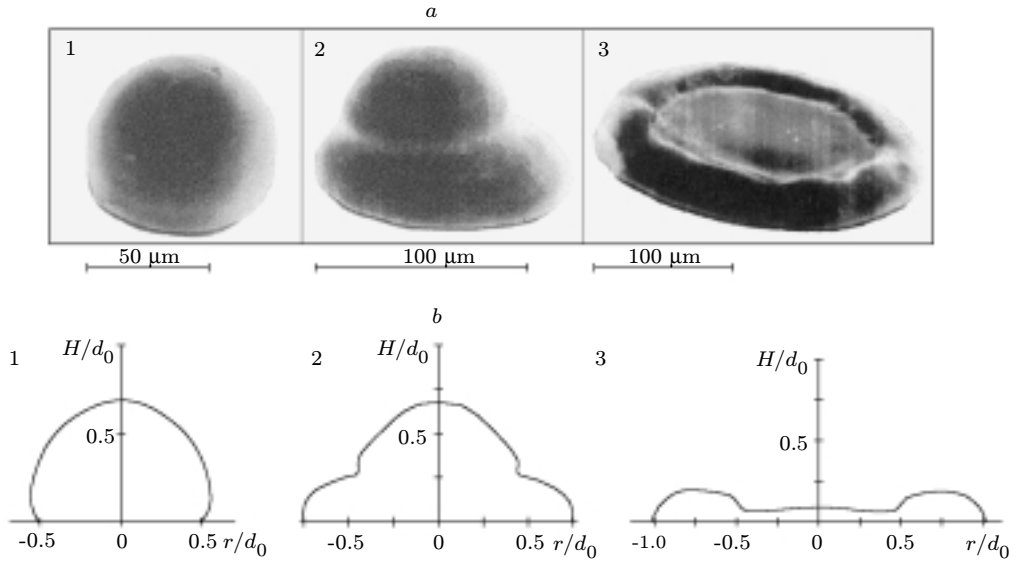

Fig. 5. Experimentally determined (a) and computed (b) shapes of the drop after its collision with the polymeric substrate ($d_0 = 68$ μm, $T_0 = 240^\circ$C, and $T_s = 50^\circ$C) for $v_0 = 0.7$ (1), 1.8 (2), and 5 m/sec.

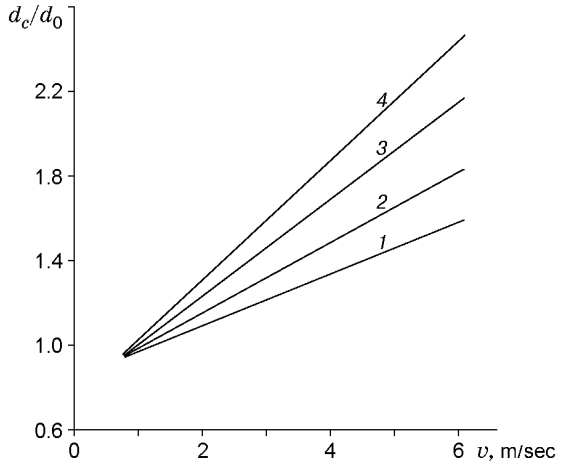

Fig. 6

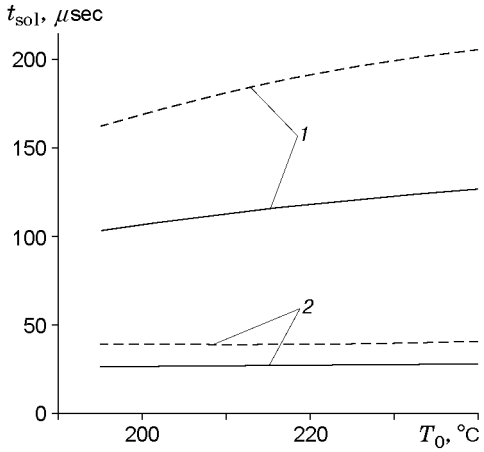

Fig. 7

Fig. 6. Relative contact-spot diameter d_c/d_0 of the solid drop versus impact velocity ($T_0 = 240^\circ$C and $T_s = 50^\circ$C) for $d_0 = 25$ (1), 40 (2), 68 (3), and 91 μm (4).

Fig. 7. Total time of drop solidification versus initial melt temperature ($T_s = 50^\circ$C) for $v_0 = 1.8$ (1) and 5 m/sec (2); the solid and dashed curves refer to $d_0 = 68$ and 91 μm, respectively.

drop (approximately 1/8 of the particle height) remains liquid. By the above-indicated time, the drop has executed three oscillations (Figs. 2 and 3a). At first, the height of the drop $H(t)$ decreases, and the liquid spreads in the radial direction. Subsequently, the direction of the fluid flow changes to the opposite one, and the top of the drop starts ascending. Then, the whole process recurs. Simultaneously, as a result of directional heat removal, the lower layers of the drop solidify, giving rise to a collar formed at the drop periphery by the radially flowing fluid. The mass of the liquid volume of the drop gradually decreases. As the mass of the melt not yet solidified decreases, the frequency of the oscillations increases (the period diminishes), and the amplitude decreases tending to zero due to the loss of the fluid-flow energy for viscous friction and work against the surface-tension force (Fig. 3a). The total solidification time of the drop in the case under consideration is 127.6 μsec.

Varlamov et al. [11] derived the following analytical relations for the linear frequency $\omega(t)$ and the number of oscillations n the liquid part of the drop executes for the total solidification time:

$$\omega(t) = \omega_0(1 - (t/t_{\rm sol})^{1/2})^{-1/2}; \tag{13}$$

$$n = (8/3)\omega_0 t_{\rm sol}. \tag{14}$$

Here $t_{\rm sol}$ is the total solidification time and ω_0 is the linear oscillation frequency of the free surface of the drop, given by the formula [14]

$$\omega_0 = (4/\pi)\sqrt{\sigma/(\rho d_0^3)}. \tag{15}$$

For $d_0 = 68$ μm and for the above-indicated values of σ and ρ, it follows from (15) that $\omega_0 = 1.47 \cdot 10^4$ sec^{-1}. Inserting this value and $t_{\rm sol} = 127.6$ μsec into (14), we find the number of executed oscillations $n = 5$. This value agrees well with the data of Fig. 3a. To compare the values calculated by formula (13) with the data of Fig. 3a, we may conveniently introduce the oscillation period $\tau_{\rm osc} = \omega_0^{-1}(1 - (t/t_{\rm sol})^{1/2})^{1/2}$. Substituting the values of ω_0 and $t_{\rm sol}$ into this formula and setting the current values of t equal to those corresponding to the maxima in the curve of Fig. 3a ($t_{\max} = 45.5$, 80, 97.4, 107.5, and 115 μsec), we obtain the analytically determined values $\tau_{\rm osc} = 43.2$, 31, 24.2, 19.4, and 15.3 μsec, whereas the numerical algorithm yields $\tau_{\rm osc} = 45.5$, 34.5, 17.4, 10.1, and 7.5 μsec.

The final shape of the drop after its complete solidification is a cone with a rounded-off vertex and corrugated (stepwise) side surface. The total number of waves on the corrugated side surface of the cone equals the number of oscillations executed by the liquid phase of the drop. The relative height and radius of the contact spot of the solid drop are 0.8 and 0.675, respectively.

If the drop impinges onto a polymeric substrate with low thermal conductivity, the total solidification time turned out to far exceed the period of drop oscillations. Moreover, these oscillations almost completely decay by the moment the crystallization begins. Therefore, the particle vertex display a regular oscillation behavior with constant frequency and decreasing amplitude (Fig. 3b). The predicted oscillation period coincides, within 6–8%, with the theoretically estimated one obtained by formula (3). The drop solidifies as a segment with a smooth surface (Fig. 4).

With increasing impact velocity, the area of the contact spot after the complete spreading of the drop increases (Fig. 5). The thickness of the solid drop and its total solidification time both decrease. For instance, at the impact velocity $v_0 = 5$ m/sec, a drop 68 μm in diameter completely spreads over the substrate for a time of 28 μsec and acquires the shape of a thin disk enclosed, in its periphery, by a ring collar (Fig. 5). The reverse flow of the fluid toward the disk center has not enough time to reach it, since the central zone of the disk has already completely solidified, and the energy of the fluid is not sufficient to overcome viscous-dissipation forces and the surface-tension force that acts from the internal boundary of the collar. For this reason, the drop after its solidification acquires the shape of a disk with a hollow in its central region. The total solidification time is 58 μsec. The height of the drop at its axis ($y = 0$) monotonically changes until the drop gets completely solidified.

Figure 6 shows the experimental and computed dependences of the relative contact-spot diameter of the solid drop on the impact velocity. Figure 7 shows the total solidification time of drops versus the initial melt overheating. It is seen from Fig. 7 that the dependences are almost linear, and the values of $t_{\rm sol}$ increase with increasing drop diameter. Waldvogel and Polikakos [2] showed that the solidification time decreases with increasing overheating (everywhere except for some temperature intervals). This phenomenon is likely caused by the too rough approximation of the effective heat capacity, related to the "smearing" of the crystallization heat over the whole temperature range of interest. In the present study, a local "smearing" in a vicinity of the phase-transition boundary was assumed, which enabled us to more adequately allow for the crystallization heat.

REFERENCES

1. D. J. Hayts, D. B. Wallace, and M. T. Boldman, "Picoliter solder droplet dispersion," *Int. J. Microcircuits Electr. Packaging*, **16**, 173–180 (1993).
2. J. M. Waldvogel and D. Polikakos, "Solidification phenomena in picoliter size solder droplet dispersion on a composite substrate," *Int. J. Heat Mass Transfer*, **40**, No. 2, 295–309 (1997).
3. F. H. Harlow and J. E. Welch, "Numerical calculation of time-dependent viscous incompressible flow of fluid with free surface," *Phys. Fluids*, **8**, 2182–2189 (1965).
4. G. Tarapaga and J. Szekely, "Mathematical modelling of the isothermal impingement of liquid droplet in spray processes," *Metall. Trans.*, **22**, 901–914 (1991).
5. A. I. Fedorchenko, "Hydrodynamic and thermophysical features of the impingement of melt drops onto solid surfaces," Author's Abstract, Doct. Dissertation in Phys.-Math. Sci., Novosibirsk (2000).
6. Z. Zhao, D. Polikakos, and J. Fukay, "Heat transfer and fluid mechanics during the collision of a liquid droplet with a substrate-I," *Int. J. Heat Mass Transfer*, **239**, 2771–2789 (1996).
7. I. V. Salli, *Crystallization under Rapid-Cooling Conditions* [in Russian], Naukova Dumka, Kiev (1972).
8. L. D. Landau and E. M. Lifshitz, *Theoretical Physics*, Vol. 6: *Hydrodynamics* [in Russian], Nauka, Moscow (1986).
9. A. A. Samarsky and B. D. Moiseenko, "A highly efficient computation scheme for the multidimensional Stefan problem," *Zh. Vychisl. Mat. Mat. Fiz.*, **5**, No. 5, 816–827 (1965).
10. P. J. Roache, *Computational Fluid Mechanics*, Hermosa, Albuquerque (1976).
11. Yu. D. Varlamov, M. R. Predtechensky, S. N. Ul'ynkin, et al., "Spreading and solidification of liquid metal droplets on a substrate: Experimental, analytic models and numerical simulation," *Int. J. Microcircuits Electronic Packaging*, **23**, No. 4, 386–392 (2000).
12. V. E. Zinov'ev, *Thermophysical Properties of Metals at High Temperatures* [in Russian], Metallurgiya, Moscow (1989).
13. G. S. Ershov and V. A. Chernyakov, *Structure and Properties of Liquid and Solid Metals* [in Russian], Metallurgiya, Moscow (1978).
14. R. Choft, J. R. Grace, and M. E. Weber, *Bubbles, Drops, and Particles*, Academic Press, New York (1978), pp. 187–188.